

Soluble triarylamine functionalized symmetric viologen for all-solid-state electrochromic supercapacitors

Yanling Zhuang¹, Weiwei Zhao¹, Longlu Wang¹, Feiyang Li¹, Weikang Wang¹, Shujuan Liu^{1*}, Wei Huang^{1,2} & Qiang Zhao^{1*}

¹ Key Laboratory for Organic Electronics and Information Displays & Jiangsu Key Laboratory for Biosensors, Institute of Advanced Materials, Nanjing University of Posts and Telecommunications, Nanjing 210023, China;

² Frontiers Science Center for Flexible Electronics & Shaanxi Institute of Flexible Electronics, Northwestern Polytechnical University, Xi'an 710072, China

Received April 7, 2020; accepted June 8, 2020; published online August 13, 2020

Electrochromic supercapacitors have drawn enormous attention due to their ability to monitor the charge and discharge processes through color changes of electroactive materials. However, there are few work on small organic molecules as active materials for all-solid-state electrochromic supercapacitors. Herein, we reported two novel multifunctional symmetric viologens (TPA-bpy and CZ-bpy), which showed different solvatochromic, electrochromic, electroluminochromic and energy storage behaviors despite their similar chemical structures. The different performances between these two viologens were attributed to the difference in the intramolecular charge transfer capability and the solubility in organic solvents. Devices containing TPA-bpy displayed faster response time and higher coloration efficiency due to the introduction of packing-disruptive and three-dimensional triarylamine groups. Moreover, devices containing TPA-bpy also showed energy storage characteristics with an obvious color change from purple to yellow. It showed a wide voltage window (2.0 V), long discharge time (230.3 s at 0.01 mA cm⁻²), and excellent cycling stability with 90% capacitance retention after 6,000 cycles. The work provides a new and convenient strategy towards the development of novel electrochromic capacitive materials.

viologen, solvatochromism, electrochromism, electroluminochromism, supercapacitors

Citation: Zhuang Y, Zhao W, Wang L, Li F, Wang W, Liu S, Huang W, Zhao Q. Soluble triarylamine functionalized symmetric viologen for all-solid-state electrochromic supercapacitors. *Sci China Chem*, 2020, 63, <https://doi.org/10.1007/s11426-020-9789-9>

1 Introduction

All-solid-state electrochromic supercapacitors have attracted immense research interests due to their ability to meet the needs of small and wearable electronic devices [1–5] and their combined performances of optical modulation and energy storage [6–10]. The optical properties can be reversibly changed by an external voltage, and the charge/discharge process is accompanied by color changes, which are dependent on different redox states (faradic processes) [11–14].

Therefore, the energy storage/release process can be quantitatively monitored by the optical transmittance and indicated by a color change [15]. These unique properties make all-solid-state electrochromic supercapacitors suitable for practical applications in cars, airplanes and buildings [10].

To date, research on electrochromic capacitive materials has mainly focused on transition metal oxides and hydroxides [16–18]. The slow switching time and poor coloring efficiency hinder the prosperous development of inorganic electrochromic supercapacitive materials [19]. Organic electrochromic supercapacitive materials, particularly con-

*Corresponding authors (email: iamsjliu@njupt.edu.cn; iamqzhao@njupt.edu.cn)

ductive polymers, have also attracted great research interest due to their excellent properties, such as easy structure modification, rich redox states, wide voltage window and high energy density. However, small organic molecules are rarely reported as electrochromic supercapacitive materials because they are difficult to simultaneously exhibit electrochromic and energy storage properties. Dicationic quaternary salts of 4,4'-bipyridine, also known as viologen, have been one of the most extensively studied electrochromic, electroluminochromic or energy storage materials due to their excellent electron-accepting capability, rich redox states, and easy tunability of the substituents [20–28]. Viologen-based electrochromic materials including small molecules, polymers and composite materials have been extensively studied [29,30]. For small molecular viologens, the color and spectral characteristics are modulated by changing the substituents on the nitrogen atoms. Conjugated polymers are obtained by introducing viologen units into the main chain or side chain, while polyviologens can be prepared by the reduction electropolymerization. Viologen-based composite materials can be acquired in a variety of ways, such as introducing viologen groups onto various nanostructured semiconductors, mixing with carbon nano-materials or self-assembling through two or more viologens. Compared with polymers and composite materials, small molecular viologens are easier to be synthesized and their photophysical properties are easier to be regulated. Therefore, rich color variations are easier to be obtained. Under electrical stimulus, the fluorescence change for electroluminochromic materials based on viologen is achieved by inserting aromatic groups between two pyridine groups, such as dithiophene, thiazolothiazole, benzene, naphthalene, anthracene and benzothiadiazole moieties [31]. However, only two kinds of fluorescence were achieved before and after the voltages are applied. For capacitors, viologens are often used as active materials together with other capacitive materials, and their capacity characteristics are rarely explored [29]. Therefore, small molecular viologens are highly desirable as the promising candidate for electrochromic, electroluminochromic and supercapacitive materials.

In this work, we have designed and synthesized two novel symmetric viologens (TPA-bpy and CZ-bpy) by incorporating electron-rich triphenylamine or carbazole moiety into 4,4'-bipyridine to be used as all-solid-state electrochromic supercapacitor materials. Although both viologens exhibited rich redox states, tunable absorption and emission properties, and interesting electrochromic and electroluminochromic performance, TPA-bpy had better performance due to the introduction of damaging packaging and three-dimensional triarylamine groups. Furthermore, TPA-bpy or CZ-bpy-containing all-solid-state electrochromic and electroluminochromic devices had excellent performance, such as rapid response time, good optical

contrast and high coloration efficiency. Importantly, all-solid-state electrochromic supercapacitors was also fabricated using TPA-bpy as the electroactive materials. The supercapacitors displayed a wide voltage window, long discharge time and excellent charging/discharging cyclic stability. To the best of our knowledge, this is the first example about small organic molecules for all-solid-state electrochromic supercapacitors.

2 Experimental

The details of general experimental sections were provided in the [Supporting Information online](#).

2.1 Synthesis and characterization of **4**

The mixture of **2** (0.18 mmol, 100 mg) and **3** (0.80 mmol, 299 mg) in solution of ethanol/deionized water (1:1, v/v, 60 mL) was refluxed for 84 h under nitrogen atmosphere. After the mixture was cooled to room temperature, the solution was filtered to remove the insoluble matters, and the filtrate was evaporated to dryness under reduced pressure. Recrystallization from methanol/ether to give a purple solid. Yields: 115 mg (68.0%). ^1H nuclear magnetic resonance, ^1H NMR (400 MHz, MeOH- d_4) δ (ppm): 9.46 (d, $J=6.8$ Hz, 4H), 8.84 (d, $J=6.4$ Hz, 4H), 7.72 (d, $J=8.8$ Hz, 4H), 7.48 (d, $J=8.4$ Hz, 4H), 7.17 (m, 12H), 1.37 (s, 36H). Electrospray ionization high-resolution mass spectrometry, ESI-HRMS (m/z): $[\text{M}]^+$ Calcd. for $\text{C}_{62}\text{H}_{68}\text{N}_4$: 868.54330, found: 434.27115. Elemental analysis: Anal. Calcd. for $\text{C}_{62}\text{H}_{68}\text{N}_4\text{Cl}_2$: C, 79.21; H, 7.29; N, 5.96. Found: C, 79.72; H, 7.15; N, 5.87%.

2.2 Synthesis and characterization of TPA-bpy

The mixture of **4** (0.12 mmol, 115 mg) and ammonium hexafluorophosphate (NH_4PF_6) (1.00 mmol, 163 mg) in solution of ethanol/deionized water (4:1, v/v, 60 mL) was stirred for 12 h at room temperature. A purple solid was obtained after filtration and recrystallization from methanol/ether. Yields: 73 mg (41.0%) ^1H NMR (400 MHz, DMSO- d_6) δ (ppm): 9.57 (d, $J=6.4$ Hz, 4H), 8.96 (d, $J=7.2$ Hz, 4H), 7.77 (d, $J=8.8$ Hz, 4H), 7.47 (d, $J=8.4$ Hz, 8H), 7.13 (d, $J=8.8$ Hz, 8H), 7.05 (d, $J=8.8$ Hz, 4H), 1.31 (s, 36H). ^{13}C NMR (100 MHz, DMSO- d_6) δ (ppm): 150.9, 148.3, 148.2, 145.3, 143.6, 134.4, 127.3, 126.9, 126.1, 126.0, 119.8, 34.5, 31.6. ^{19}F NMR (377 MHz, DMSO- d_6) δ (ppm): -70.13 (d, $J=711.6$ Hz). ESI-HRMS (m/z): $[\text{M}]^+$ Calcd. for $\text{C}_{62}\text{H}_{68}\text{N}_4$: 868.54330, found: 434.27121. Elemental analysis (%): Anal. Calcd. for $\text{C}_{62}\text{H}_{68}\text{N}_4\text{P}_2\text{F}_{12}$: C, 64.24; H, 5.91; N, 4.83. Found: C, 64.40; H, 6.05; N, 4.91.

2.3 Synthesis and characterization of 7

The mixture of **3** (0.18 mmol, 100 mg) and **6** (0.80 mmol, 297 mg) in solution of ethanol/deionized water (5:1, v/v, 60 mL) was refluxed under nitrogen atmosphere for 84 h. After the mixture was cooled to room temperature, the solution was filtered to remove the insoluble matters, and the filtrate was evaporated to dryness under reduced pressure. Recrystallization from methanol/tetrahydrofuran to obtain a red solid. Yields: 101 mg (60.0%). ^1H NMR (400 MHz, MeOH- d_4) δ (ppm): 9.84–9.70 (m, 4H), 9.13–8.99 (m, 4H), 8.34–8.20 (m, 8H), 8.12 (d, $J=8.0$ Hz, 4H), 7.63–7.52 (m, 8H), 1.51 (s, 36H). ESI-HRMS (m/z): $[\text{M}]^+$ Calcd. for $\text{C}_{62}\text{H}_{64}\text{N}_4$: 868.51200, found: 864.50952. Elemental analysis (%): Anal. Calcd. for $\text{C}_{62}\text{H}_{64}\text{N}_4\text{Cl}_2$: C, 79.55; H, 6.89; N, 5.99. Found: C, 78.83; H, 6.88; N, 6.73.

2.4 Synthesis and characterization of CZ-bpy

The mixture of **7** (0.11 mmol, 101 mg) and NH_4PF_6 (1.00 mmol, 163 mg) in solution of ethanol/deionized water (5:1, v/v, 60 mL) was stirred for 12 h at room temperature. A fuchsia solid was obtained after filtration and washing with ethanol and water. Yields: 87 mg (55%). ^1H NMR (400 MHz, DMSO- d_6) δ (ppm): 9.87 (d, $J=6.4$ Hz, 4H), 9.19 (d, $J=6.8$ Hz, 4H), 8.41–8.36 (m, 4H), 8.28 (d, $J=8.8$ Hz, 4H), 8.16 (d, $J=8.4$ Hz, 4H), 7.58 (d, $J=8.8$ Hz, 4H), 7.48 (d, $J=8.8$ Hz, 4H), 1.46 (s, 36H). ^{13}C NMR (100 MHz, DMSO- d_6) δ (ppm): 149.6, 146.1, 144.0, 140.8, 140.3, 138.3, 127.9, 127.2, 127.1, 124.5, 123.8, 117.3, 109.5, 35.0, 32.0. ^{19}F NMR (377 MHz, DMSO- d_6) δ (ppm): -70.12 (d, $J=711.6$ Hz). ESI-HRMS (m/z): $[\text{M}]^+$ Calcd. for $\text{C}_{62}\text{H}_{64}\text{N}_4$: 868.51200, found: 864.50958. Elemental analysis (%): Anal. Calcd. for $\text{C}_{62}\text{H}_{64}\text{N}_4\text{P}_2\text{F}_{12}$: C, 64.47; H, 5.58; N, 4.85. Found: C, 63.35; H, 5.57; N, 4.92.

2.5 Fabrication of all-solid-state electrochromic and electroluminescent devices and supercapacitors

Electrochromic and electroluminescent film was prepared by dropping the TPA-bpy or CZ-bpy and polyvinylpyrrolidone (PVP, film-former, mass ratio=1:1) in acetonitrile solution onto indium-doped tin oxide (ITO)-coated glass. The film was vacuum dried at 80 °C for 24 h for the complete curing. A transparent gel electrolyte was obtained by mixing polymethyl methacrylate (PMMA, M_w : 120,000, 0.7 g), LiClO_4 (0.3 g) and propylene carbonate (PC, 3.0 g) in dry acetonitrile (2 mL). The mixture was stirred rapidly at 50 °C until a gelation occurred. The gel electrolyte was coated on a new ITO-coated glass by a pulling method. The above two ITO-coated glasses were bonded together and dried in a vacuum oven at 80 °C for 12 h to obtain all-solid-state electrochromic and electroluminescent devices and

supercapacitors. The film thickness of the devices was measured by the scanning electron microscope (SEM) and the average film thickness is 17.97 μm . Cross-sectional SEM images of the devices are shown in Figure S1 (Supporting Information online).

2.6 Related calculations for all-solid-state supercapacitors

The specific capacitance (C) is calculated from the galvanostatic charge/discharge (GCD) curves according to the following equation:

$$C = \frac{It}{\Delta V} \quad (1)$$

The energy density (E) and power density (P) are calculated from the following equations, respectively:

$$E = \frac{1}{2} \times C \times (\Delta V)^2 \times \frac{1}{3600} \quad (2)$$

$$P = 3600 \times \frac{E}{t} \quad (3)$$

where I is the applied current, t is the discharge time, ΔV is the actual potential window excluding the IR drop.

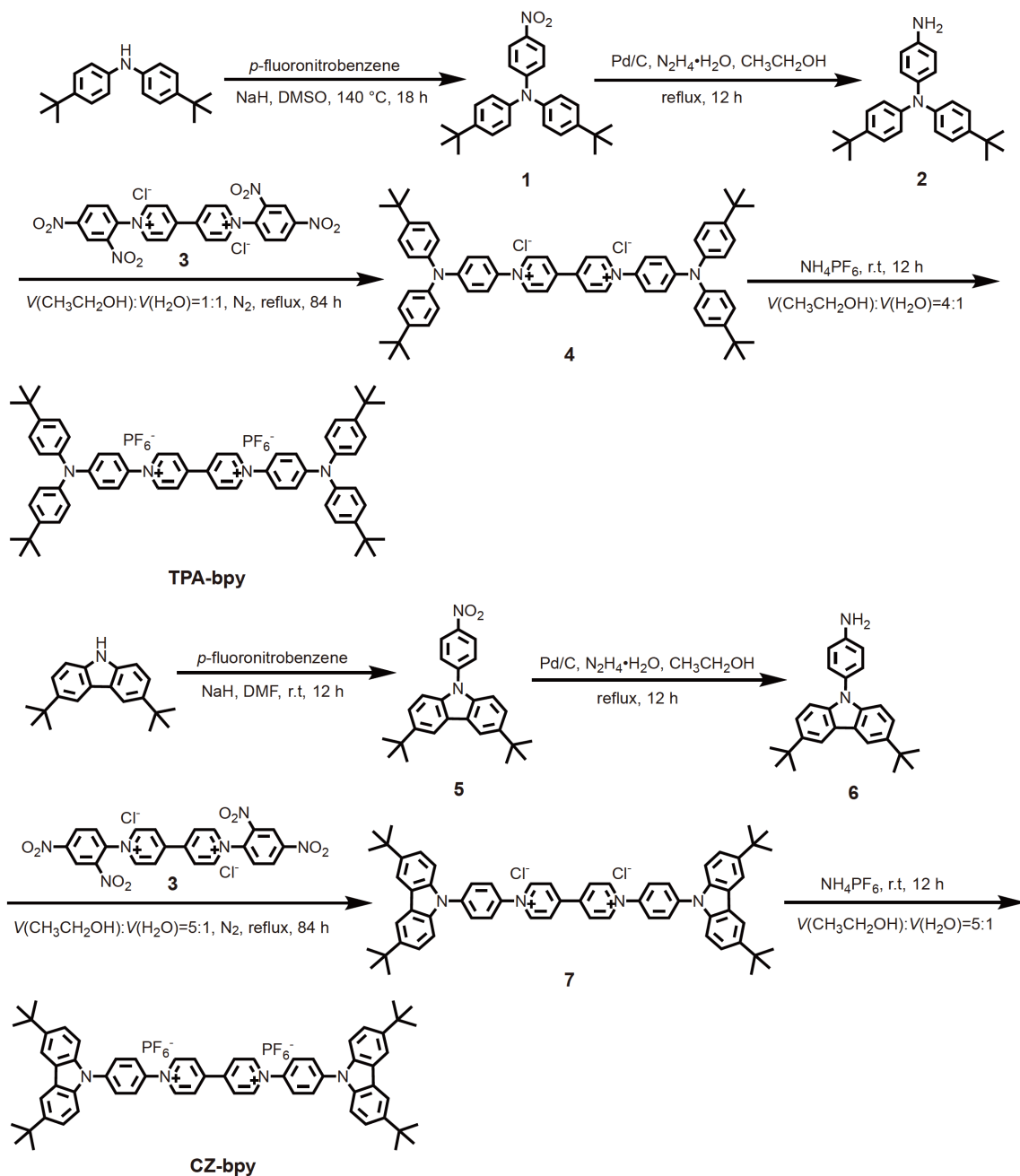
3 Results and discussion

3.1 Synthesis and characterization of viologen derivatives

The synthetic procedures of TPA-bpy and CZ-bpy are shown in Scheme 1 in three steps. Firstly, the intermediate **3** was obtained by the Zincke reaction between 1-chloro-2,4-dinitrobenzene and 4,4'-bipyridine. Next, **4** and **7** were respectively synthesized by refluxing the intermediate **3** and the corresponding aromatic amine **2** or **6** in a mixed solvent of ethanol and water for 84 h under nitrogen atmosphere. At last, **4** and **7** were respectively stirred with NH_4PF_6 in a mixed solvent of water and ethanol at room temperature for 12 h to obtain target products TPA-bpy and CZ-bpy. Among them, compounds **1–3**, **5** and **6** were synthesized according to the literature reports [32–34]. The new intermediates and viologen derivatives were characterized by NMR (^1H NMR, $^{13}\text{C}\{^1\text{H}\}$ NMR and $^{19}\text{F}\{^1\text{H}\}$ NMR), ESI-HRMS and elemental analysis. The purpose of introducing a large *tert*-butyl substituent at the active site of the triphenylamine and carbazole units was to increase the solubility and avoid electrochemical polymerization of the viologens. Ion exchange was used to further improve the solubility of TPA-bpy and CZ-bpy in organic solvents.

3.2 Photophysical and electrochemical properties of viologen derivatives

The optical properties of TPA-bpy and CZ-bpy were studied



Scheme 1 Synthetic routes of TPA-bpy and CZ-bpy.

by ultraviolet-visible (UV-Vis) absorption spectroscopy as shown in Figure 1(a). Both TPA-bpy and CZ-bpy have two absorption peaks. Among them, the absorption peak around 300 nm is the characteristic absorption of viologen, and the maximum absorption wavelength around 500 nm can be attributed to charge transfer transition from triphenylamine or carbazole moieties to 4,4'-bipyridine. In addition, the maximum absorption peak of TPA-bpy is red shifted by about 40 nm from that of CZ-bpy. This change in absorption is accompanied by an increase in the energy gap from 1.80 eV (TPA-bpy) to 2.03 eV (CZ-bpy) and can be explained by the

stronger electron donating ability of the triphenylamine than that of the carbazole group (Table S1, Supporting Information online). Figure 1(b) exhibits the emission spectra of TPA-bpy and CZ-bpy. The maximum emission peaks of TPA-bpy and CZ-bpy are about 600 and 425 nm, respectively. The emission wavelength of TPA-bpy is significantly red-shifted compared with that of CZ-bpy, which indicates that the intramolecular charge transfer capability of TPA-bpy is greater than that of CZ-bpy. This experimental phenomena can be further confirmed by theoretical calculations. The frontier orbital distributions of TPA-bpy and CZ-bpy are

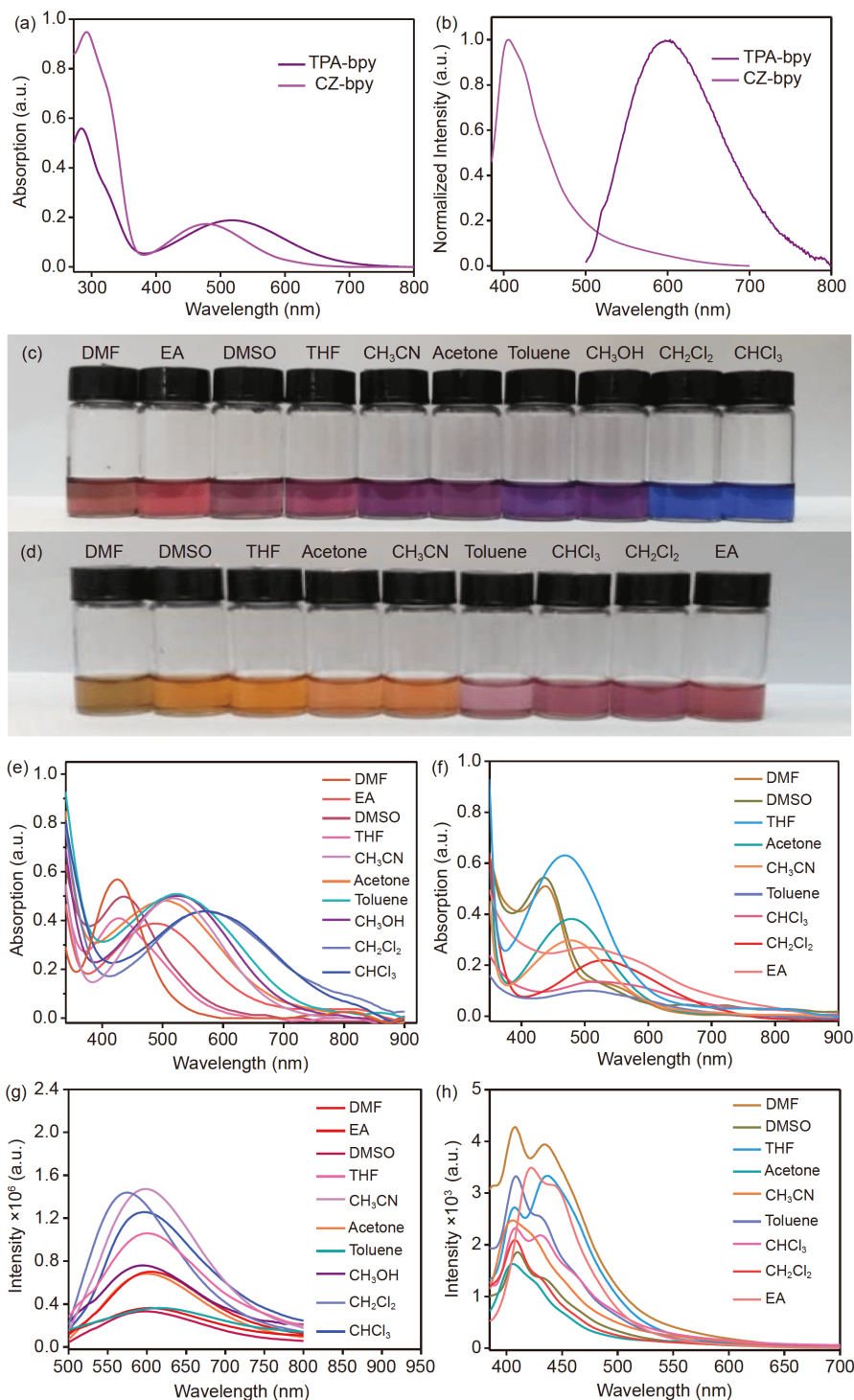


Figure 1 (a) UV-Vis absorption and (b) emission spectra of TPA-bpy and CZ-bpy (1×10^{-5} M) in dry acetonitrile at 298 K. Photographs of (c) TPA-bpy and (d) CZ-bpy (2.5×10^{-4} M) in different solvents. UV-Vis absorption spectra of (e) TPA-bpy and (f) CZ-bpy (1×10^{-5} M) in different solvents at 298 K. Emission spectra of (g) TPA-bpy and (h) CZ-bpy (1×10^{-5} M) in different solvents at 298 K (color online).

shown in Section 3.3. The highest occupied molecular orbital (HOMO) of the two viologen derivatives are distributed on the triphenylamine or carbazole groups, respectively, while the lowest unoccupied molecular orbital (LUMO) are mainly distributed on the bipyridyl group and the benzene rings attached to the bipyridine, indicating the possible in-

tramolecular charge transfer transition.

Triphenylamine and carbazole groups display excellent hole-transport properties, and are typically incorporated into electrochromic materials because lone electron pairs of the nitrogen atoms on them can be effectively oxidized to a cationic free radical state, which is usually accompanied by

the color change [34–38]. Moreover, triphenylamine moiety can prevent intermolecular aggregation due to its non-planar structure such that the solubility and film-forming property of TPA-bpy can be improved [34–37]. Therefore, the solvatochromic, electrochromic, electroluminochromic and energy storage behaviors of TPA-bpy are superior to those of CZ-bpy.

Interestingly, both TPA-bpy and CZ-bpy showed solvatochromic behaviors, but TPA-bpy has better performance due to the introduction of damaging pack aging and three-dimensional triarylamine groups. In order to better demonstrate the solvatochromic properties, TPA-bpy and CZ-bpy were first studied in various solvents with different polarities. The colors of TPA-bpy in different solvents were light pink, purple, violet and blue, while CZ-bpy in different solvents only showed orange and light pink (Figure 1(c, d)). The UV-Vis absorption spectra and absorption maxima of two viologen derivatives in different solvents are shown in Figure 1(e, f) and Table S2, respectively. The maximum absorption wavelengths of TPA-bpy are ranged from 425 to 572 nm, and those of CZ-bpy are about 438–535 nm. In addition, the emission spectra of TPA-bpy and CZ-bpy in different solvents were further investigated as shown in Figure 1(g, h). All emission spectra for TPA-bpy are similar without significant red- or blue-shift, while CZ-bpy in other solvents has two emission peaks except for acetone and acetonitrile and the emission peaks mainly centered at 408–435 nm, indicating no correlation between emission spectra and solvent polarity. The solvatochromism of TPA-bpy and CZ-bpy indicates that the solvents have a greater influence on the ground state dipole moment and little effect on the excited-state dipole moment [39,40].

The cyclic voltammetry (CV) curves of TPA-bpy and CZ-bpy are shown in Figure 2(a, b), and the electrochemical data are summarized in Table S2. Both TPA-bpy and CZ-bpy underwent reversible two-electron reduction and single-electron oxidation. Scheme S1 (Supporting Information online) demonstrates the proposed reduction and oxidation reaction sequence for TPA-bpy and CZ-bpy for producing different anionic and cationic substances, which can be

confirmed by the reported literatures [23–25,34–37]. The two pairs of redox peaks obtained during the cathode scan can be attributed to the two one-electron redox processes of the 4,4'-bipyridine units, corresponding to the generation of radical cationic and neutral species, respectively. The formation of bi-radical cationic substances during oxidation of the triphenylamine and carbazole units resulted in redox waves observed by TPA-bpy and CZ-bpy during the anode scan. Interestingly, compared to CZ-bpy ($E_{1/2}^{\text{Red1}} = -0.47$ V, $E_{1/2}^{\text{Red2}} = -0.76$ V, $E_{1/2}^{\text{Ox}} = 1.10$ V), TPA-bpy has lower redox potentials ($E_{1/2}^{\text{Red1}} = -0.57$ V, $E_{1/2}^{\text{Red2}} = -0.91$ V, $E_{1/2}^{\text{Ox}} = 0.75$ V). This can be explained by the fact that lone electron pairs of the nitrogen atoms on carbazole groups are preferably located in the coplanar ring, such that the oxidation potential of the carbazole moiety is higher than that of the triphenylamine group, resulting in more difficult reduction of the bipyridyl group on CZ-bpy [37].

3.3 Theoretical calculations

Density functional theory (DFT) calculations have been performed for TPA-bpy and CZ-bpy in order to further confirm the experimental findings (Figure 3). The calculated results are in consistent with the trends observed by UV-Vis absorption spectra and CV curves (Table S1). Two viologen derivatives exhibit similar and clearly visible HOMO and LUMO distributions. Because of the donor-character of the triphenylamine or carbazole substituents, the HOMOs are mainly located in the donor parts of the viologens. The LUMOs are corresponding to varying degrees of delocalization on nitrogen atom of triphenylamine or carbazole groups and the *N*-aryl substituents. For the radical cationic states, the LUMOs clearly show electron density contribution from the *N*-aryl substituents and HOMOs are distributed on the entire π^* -system, which indicates a strong delocalization of the molecules. Poor delocalization is exhibited for the neutral states because their HOMOs and LUMOs are mainly distributed on the *N*-aryl substituents and the benzene rings attached to the *N*-aryl substituents. However, the LUMOs and HOMOs for bi-radical cationic state are still mainly

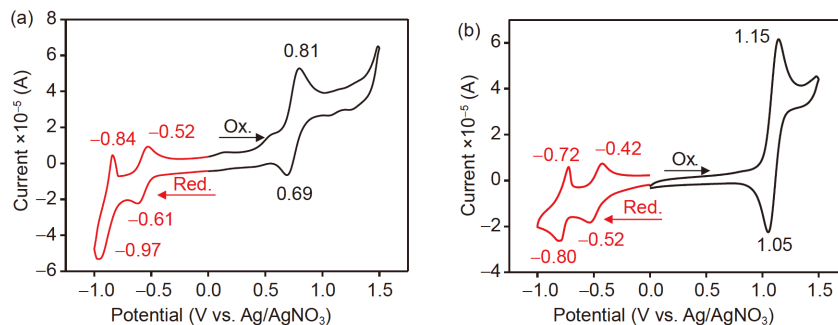


Figure 2 Cyclic voltammetry curves of (a) TPA-bpy, (b) CZ-bpy recorded in anhydrous acetonitrile (0.1 M *n*Bu₄NPF₆) at 298 K using a glassy carbon working electrode at a sweep rate of 100 mV s⁻¹ (color online).

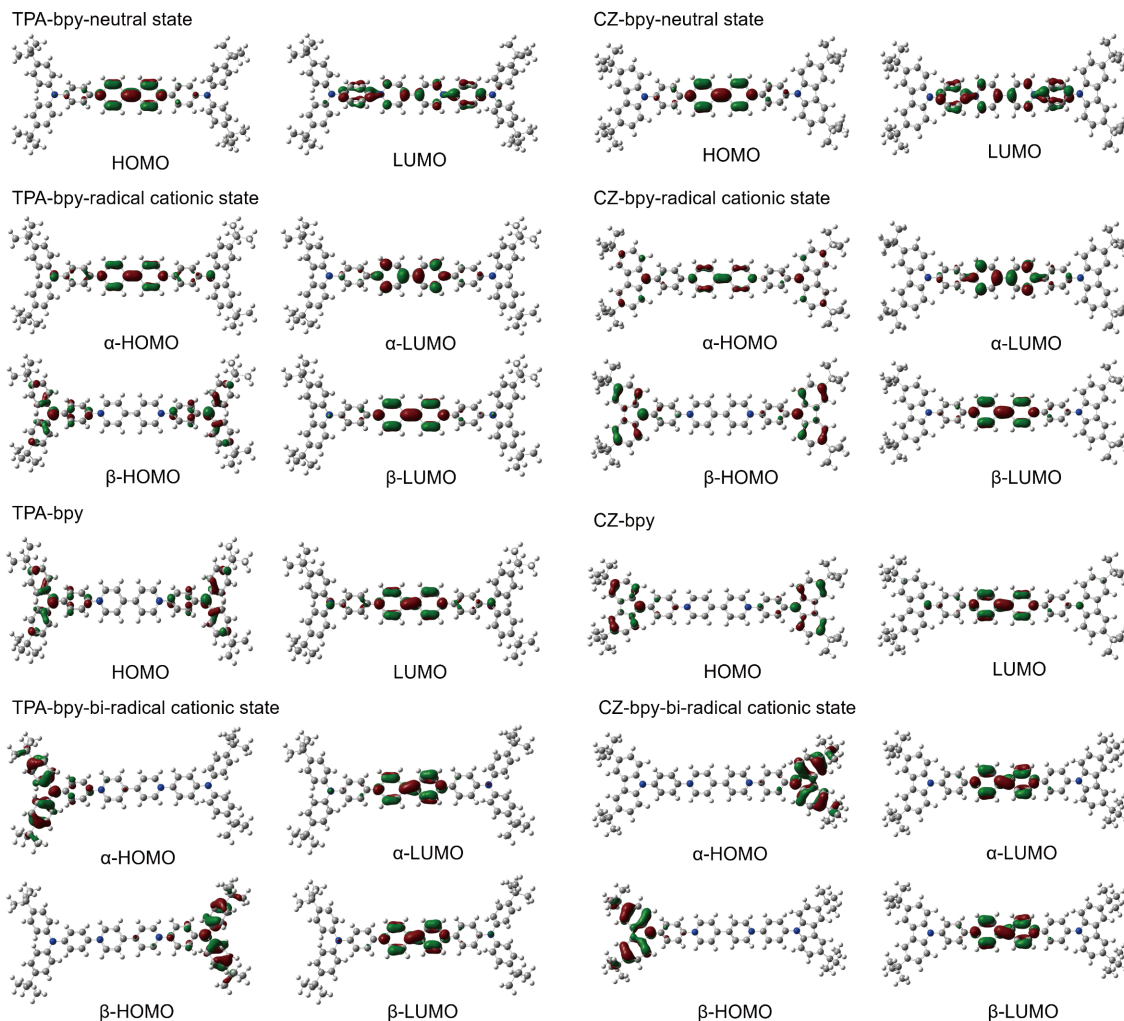


Figure 3 HOMO and LUMO distributions of TPA-bpy and CZ-bpy (color online).

distributed on the *N*-aryl substituents and triphenylamine or carbazole groups, respectively. The different electron density distributions and intramolecular charge transfer capability exhibited by the different oxidation states of the two molecules result in their rich color and luminescence changes under electrical stimulus.

3.4 Chemical reduction of viologen derivatives

It is recognized that electrochromism was due to the reduction of 4,4'-bipyridine and the oxidation of triphenylamine or carbazole groups in two viologens [37,41,42]. Therefore, the discoloration and luminescence responses of TPA-bpy and CZ-bpy towards different reducing agents including NaBH₄, NaHS, KI, and KBr have been studied. Interestingly, TPA-bpy and CZ-bpy underwent color and luminescence change only in the presence of the reducing agent NaBH₄ at room temperature. Before NaBH₄ was added, the TPA-bpy acetonitrile solution was purple and showed orange emis-

sion. After 0.1 eq. of NaBH₄ was added, both the solution and luminescence colors changed to yellow, indicating that TPA-bpy has been reduced to radical cationic species. When 0.2 eq. of NaBH₄ was added, both the solution and luminescence colors changed to pale yellow and blue, respectively, indicating that TPA-bpy was further reduced to neutral species. There was no significant change in the color, and only the luminescence intensity increased after the excess NaBH₄ was dropped (Figure 4(a)). The UV-Vis absorption and emission spectra of TPA-bpy with the addition of NaBH₄ are shown in Figure 4(b, c). Unlike TPA-bpy, the solution and luminescence colors of CZ-bpy changed slightly when NaBH₄ was added. Moreover, when 0.2 eq. of NaBH₄ was added, the solution color changed from orange to yellow, and the luminescent color did not change significantly, but the intensity decreased. The solution became light yellow and the luminescent intensity was enhanced by adding 0.4 eq. of NaBH₄. The solution changed from light yellow to colorless, and the emission intensity continued to

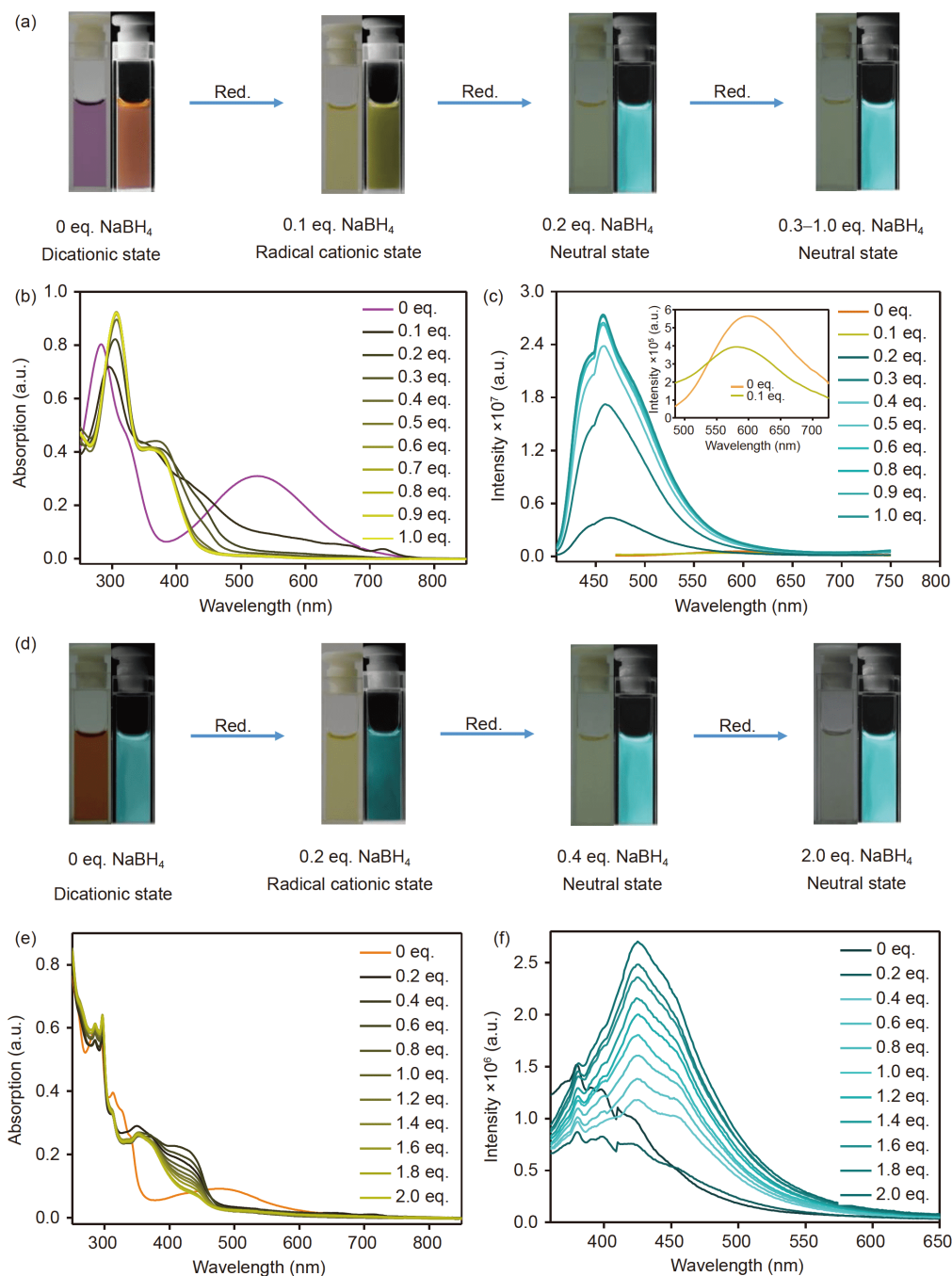


Figure 4 (a) Photograph of TPA-bpy (2.5×10^{-4} M) with the addition of NaBH_4 in anhydrous acetonitrile at 298 K. (b) UV-Vis absorption and (c) emission spectra of TPA-bpy (1×10^{-5} M) with the addition of NaBH_4 in anhydrous acetonitrile at 298 K. (d) Photographs of CZ-bpy (2.5×10^{-4} M) with the addition of NaBH_4 in anhydrous acetonitrile at 298 K. (e) UV-Vis absorption and (f) emission spectra of CZ-bpy (1×10^{-5} M) with the addition of NaBH_4 in anhydrous acetonitrile at 298 K (color online).

increase when an excess of NaBH_4 was dropped (Figure 4 (d)). This change process can be proven by the UV-Vis absorption and emission spectra of CZ-bpy with the addition of NaBH_4 (Figure 4(e, f)). The above results indicate that TPA-bpy is more easily reduced by NaBH_4 than CZ-bpy. Fluorescence quantum yields (Φ) of two viologen with different redox states in anhydrous acetonitrile at 298 K are shown in Table S3.

3.5 Fabrication and performance of all-solid-state electrochromic and electroluminochromic devices

On the basis of the above results, we have successfully prepared the bi-functional electrochromic and electroluminochromic devices using TPA-bpy or CZ-bpy as electroactive materials, respectively. The schematic diagram of the devices is shown in Figure S2. For the TPA-bpy-con-

taining devices, the film was purple and displayed orange emission before the external voltage was applied. Both the film and luminescence colors gradually turned to yellow due to the formation of radical cationic species when a voltage of -1.2 V was applied (Figure 5(a)). Furthermore, due to the accumulation of neutral substances, the film and the luminescent colors changed to pale yellow and blue, respectively, by applying a higher voltage of -1.6 V (Figure 5(a)). In addition, the yellow film and blue emission were observed at an external electrical bias of 2.0 V (Figure 5(a)). The corresponding UV-Vis absorption and emission spectra of the TPA-bpy-containing bi-functional devices at different voltages were further explored (Figure 5(b–e)). Prior to the voltage applied, two absorption peaks were observed for TPA-bpy-containing devices. The absorption peaks around 300 and 500 nm had a red shift of about 40 nm and slight blue shift, respectively, compared to those in acetonitrile. At an external potential bias of -1.2 V, two absorption peaks had slightly red and blue shifts, respectively. The absorption peak around 300 nm was still red-shifted, while that at 500 nm disappeared at a voltage of -1.6 or 2.0 V. The emission spectra of the devices under different negative

pressures are similar to those in the above chemical reduction experiment.

The UV-Vis transmittance spectra of the TPA-bpy-containing bi-functional devices under different applied voltages are shown in Figure 5(f, g). At the voltages of -1.2 and -1.6 V, the TPA-bpy film had optical transmittance changes ($\Delta T\%$) of 46% and 52% at 411 nm, respectively, while a higher optical contrast (76%) was obtained at 380 nm at an external potential bias of 2.0 V. Figure 6(a) describes the optical transmittance at 411 nm as a function of time by applying square-wave potential steps between 0 and -1.2 V with a resident time of 20 s for the TPA-bpy film. The color switching time is defined as the time required to reach 90% of the total change in transmittance after switching the potential, because it is difficult to visually observe any further color changes after this point [35–37,42]. The coloring and bleaching times were 4.5 and 2.2 s, respectively. (Figure 6 (b)). Figure S5a displays a very small change in $\Delta T\%$ as the potential square wave resonance number increases, which indicated that the TPA-bpy film has high stability upon reduction to radical cationic species. When the voltage was set between 0 and -1.6 V, the coloring and bleaching times of

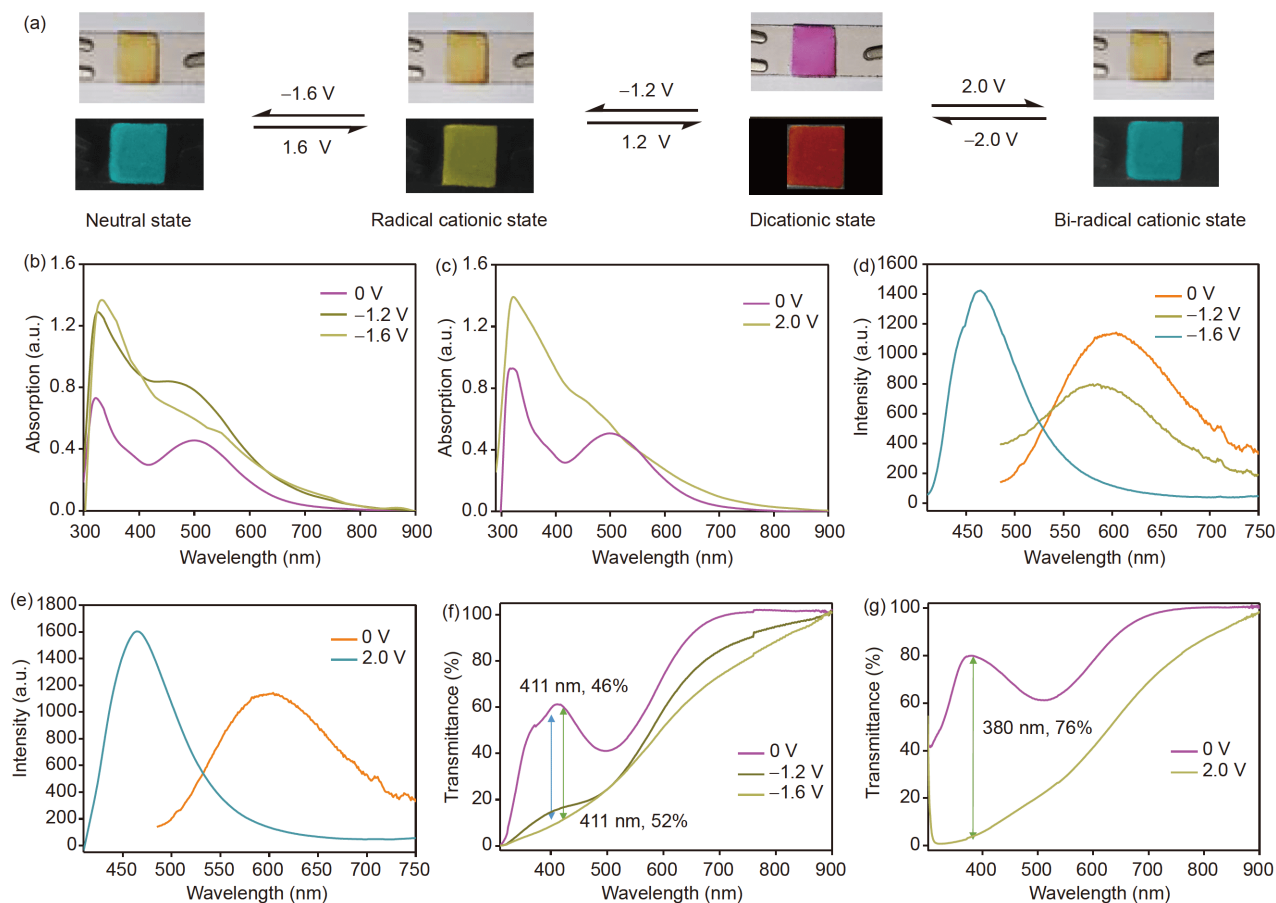


Figure 5 (a) Photographs, (b, c) UV-Vis absorption, (d, e) emission and (f, g) transmittance spectra of the TPA-bpy-containing bi-functional devices under different voltages (color online).

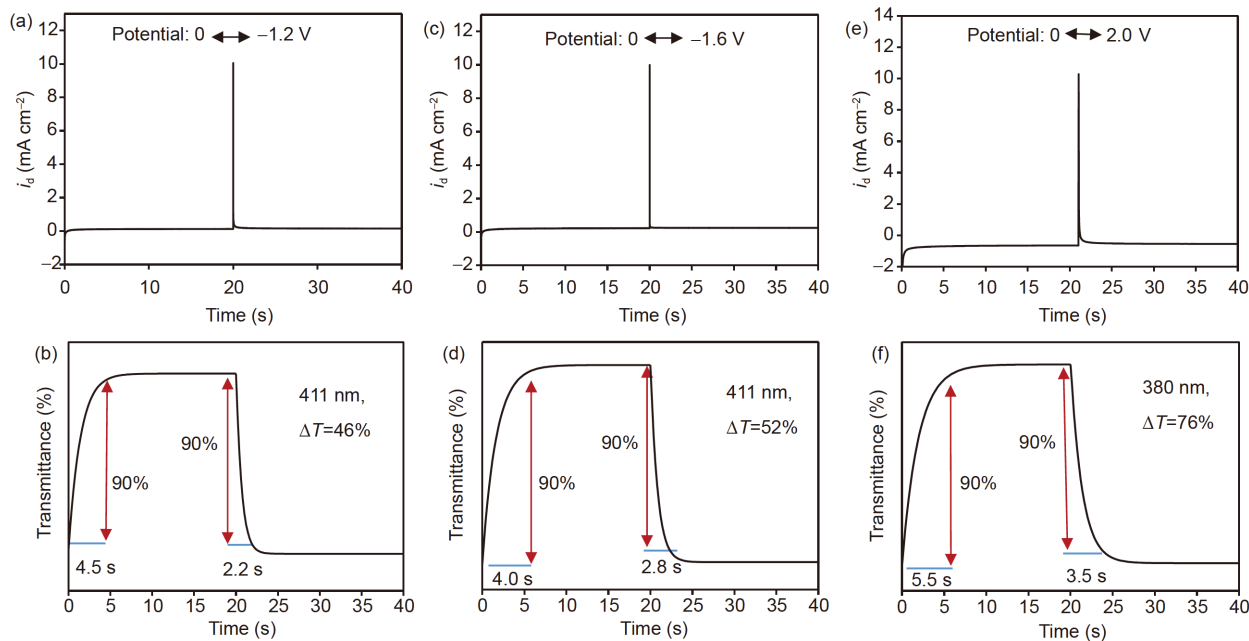


Figure 6 (a, c, e) Current consumption and (b, d, f) electrochromic/electroluminochromic switching studies for the TPA-bpy-containing bi-functional devices monitored at $\lambda_{\max}=411, 411$ and 380 nm, respectively, at external applied potentials with a residence time of 20 s (color online).

the devices were 4.0 and 2.8 s, respectively (Figure 6(c, d)). However, $\Delta T\%$ had a large loss after 1,600 s as the number of potential square wave cycles increased, which meant that the reduced stability was exhibited in the neutral state of the TPA-bpy film (Figure S5(a)). The bi-functional devices required 5.5 s for coloring and 3.5 s for bleaching by applying square-wave potential steps between 0 and 2.0 V with a resident time of 20 s at 380 nm (Figure 6(e, f)). Moreover, $\Delta T\%$ hardly changed as the number of potential square wave cycles increased, which also represented that the TPA-bpy film had high stability upon oxidation to bi-radical cationic species. Coloration efficiency (CE, η) can be calculated by the equation of $\eta = \Delta OD / Q$, which is a measurement of the power efficiency of a dual-functional device, where Q is the injected/extracted charge per unit electrode area (mC cm^{-2}) and obtained by integrating Figure 6(a, c, e), and ΔOD is the change in absorbance at a specific wavelength maximum at different redox states [35–37,42]. The high CE values of radical cationic state, neutral state and bi-radical cationic state of the devices containing TPA-bpy were calculated to be 171, 250 and $294 \text{ cm}^2 \text{ C}^{-1}$, respectively (Table S4).

For the CZ-bpy-containing bi-functional devices, both film and the luminescent color changes can also be achieved under different applied voltages, but the change in luminescent colors were not as rich as that of the TPA-bpy-containing devices. Moreover, the CZ-bpy-containing devices needed a higher applied voltage when the same redox state as the TPA-bpy-containing devices was obtained. More specifically, the film was orange and exhibited blue emission

before an electrical bias was applied. When the radical cationic species was formed at the voltage of -1.6 V, the film color changed from orange to yellow, whereas the luminescence did not change significantly, but the intensity was slightly reduced by the naked eye (Figure S3(a)). Further increasing the potential to -2.0 V, both the film and luminescence colors did not change much, but the luminescence intensity increased by the naked eye, indicating the formation of neutral substances (Figure S3(a)). When the applied voltage was 2.4 V, the film changed from orange to yellow and the luminescence was still blue, but the luminescence intensity increased (Figure S3(a)). The UV-Vis absorption and emission spectra of the CZ-bpy-containing bi-functional devices at different voltages had also been studied (Figure S3 (b–e)). Two absorption peaks at about 400 and 600 nm were obtained for the CZ-bpy-containing devices prior to the voltage was applied, and both showed a red shift of about 100 nm compared to the corresponding peak in the acetonitrile solution. At -1.6 V, the peaks had a blue shift of approximately 20 and 50 nm, respectively. However, at an external electrical bias of -2.0 V, the absorption peak around 400 and 600 nm continued to be blue-shifted and disappeared, respectively. The peaks had a blue shift of approximately 15 and 100 nm, respectively, at a voltage of 2.4 V. The emission spectra of the CZ-bpy-containing devices at different voltages were consistent with those of chemical reduction experiment.

The corresponding UV-Vis transmittance spectra of the CZ-bpy-containing devices at different voltages are shown in Figure S3(f, g). The film had a high optical contrast of up to

55% at 376 nm at -1.6 V, 79% at 365 nm at -2.0 V, and 64% at 384 nm at 2.4 V, respectively. The optical transmittance at 376, 365 and 384 nm as a function of time was studied by applying square-wave potential steps between 0 and -1.6 V, 0 and -2.0 V, 0 and 2.4 V, respectively, with a resident time of 20 s for the CZ-bpy film (Figure S4). The three different redox states of the CZ-bpy film acquired coloring times of 5.5, 16.6 and 5.8 s, respectively, and the fading times were 2.7, 9.3 and 3.0 s, respectively. The electrochromic and electroluminochromic switching studies of the three redox states of the CZ-bpy film are shown in Figure S5(b). As the number of potential square wave cycles increased to 100 cycles, $\Delta T\%$ in 0– 2.4 V had slight fluctuation, and that in 0– 1.6 V and 0– 2.0 V repeated well, indicating that the CZ-bpy film had excellent stability in the reduction to radical cationic and neutral species. The CE values of radical cationic, neutral and bi-radical cationic states of the devices containing CZ-bpy were calculated to be 151, 216 and $206 \text{ cm}^2 \text{ C}^{-1}$, respectively (Table S4). The reasons for the difference in performance between the two bi-functional devices may be as follows: (1) TPA-bpy has a higher intramolecular charge transfer capability than CZ-bpy, so the devices containing TPA-bpy have lower driving voltages; (2) introducing packing-disruptive and three-dimensional triarylamine groups into 4,4'-bipyridine not only resulted in the enhancement of solubility (Table S5), but also avoided concentration quenching effectively due to π - π interactions among TPA-bpy molecules, which makes TPA-bpy exhibit richer color changes under electrical stimulus [35–37].

3.6 Fabrication and performance of all-solid-state electrochromic supercapacitors

Based on the above research on electrochromic and electroluminochromic bi-functional devices, the devices containing TPA-bpy or CZ-bpy may be referred to as pseudocapacitors. The study found that the devices containing TPA-bpy had pseudocapacitive performance, while the CZ-bpy film did not have constant current charge and discharge properties, which were attributed to its poor solubility and film formation properties resulted from its more planar structure [35–37]. For the TPA-bpy-based supercapacitors, the CV curves exhibited two reversible redox processes at different scan rates (5 to 200 mV s^{-1} , Figure 7(a)) from 0 to 2.0 V, which were related to the reversible two electron gain and loss processes of the acceptor 4,4'-bipyridine [43]. As the scan rate increased, the oxidation and reduction peaks moved to the more positive and negative positions of the potential, respectively. Moreover, the well-defined redox peaks were still maintained even at the high scanning rate of 200 mV s^{-1} , indicating that the supercapacitors had low internal resistance, good electrochemical capacitive nature and fast charge transfer [44]. The pseudocapacitive behaviors of the devices containing TPA-bpy were further investigated by GCD curves (Figure 7(b)) at various current densities, in which the GCD curves were nonlinear, indicating the presence of redox reactions from TPA-bpy. The upward and downward lines correspond to the charging and discharging processes, respectively, which were related to the mutual

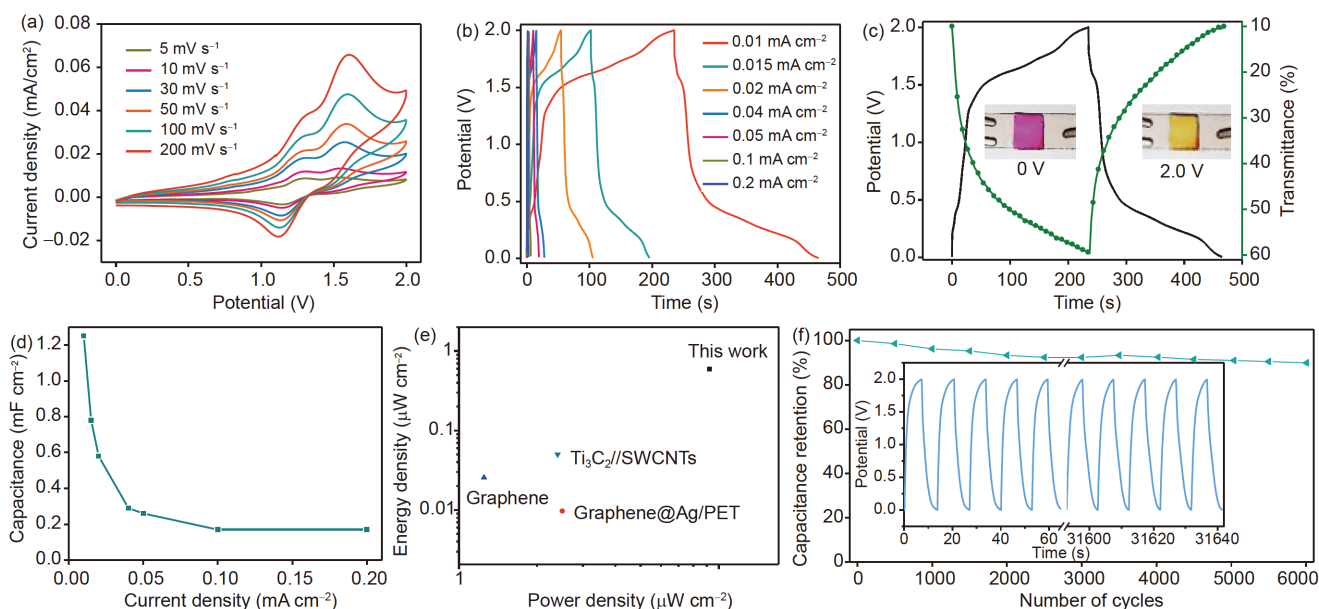


Figure 7 (a) CV curves of the supercapacitors containing TPA-bpy under different scan rates in the potential range of 0–2.0 V. (b) GCD curves of the supercapacitors containing TPA-bpy collected at various current densities. (c) GCD curves at 0.01 mA cm^{-2} in the potential range of 0–2.0 V and corresponding *in-situ* transmittance change measured at 411 nm for the supercapacitors containing TPA-bpy. Inset: photographs of the supercapacitors containing TPA-bpy under various energy storage levels, 0 and 2.0 V. (d) Areal capacitance obtained from GCD curves. (e) Energy and power density of the solid-state supercapacitors with a comparison with the previously reported devices. (f) Cycling stability of the supercapacitors at 0.04 mA cm^{-2} . Inset: the first and last 5 cycles of the supercapacitors (color online).

conversion between different redox states in the TPA-bpy film. As TPA-bpy film simultaneously functions in the electrochromic and energy storage applications and shares the same electrochemical process in the same electrolyte, the GCD curve at 0.01 mA cm^{-2} and the corresponding *in situ* transmittance change at 411 nm were explored (Figure 7(c)). During the charging process, TPA-bpy was first reduced to radical cationic species and then reduced to neutral substances with the film color changing from purple to yellow (Figure 7(c)). The fully charged state was obtained at 2.0 V, and the film was still yellow. The film gradually turned to be purple during the discharging process. The electrochromic supercapacitors exhibited an optical contrast of $\sim 50\%$ between the charged (2.0 V) and discharged (0 V) states at 411 nm. The areal capacitances (C) reached 1.25 mF cm^{-2} at 0.01 mA cm^{-2} (Figure 7(d)), which is higher than electrochromic supercapacitors and pseudocapacitors based on polymers or transition metal oxides in the literatures (Table S6). Additionally, the achieved highest energy density was $0.59 \text{ } \mu\text{Wh cm}^{-2}$ at a power density of $9.21 \text{ } \mu\text{W cm}^{-2}$, which is higher than the previously reported devices (Figure 7(e)) [45–47]. Meanwhile, the devices delivered a remarkable volumetric capacitance of 69.46 mF cm^{-3} at a current density of 0.57 mA cm^{-3} and an energy density of 0.03 mWh cm^{-3} with a power density of 0.51 mW cm^{-3} . The cycling stability was tested by GCD curve at 0.04 mA cm^{-2} . A 90% capacitance retention was acquired after 6,000 charge/discharge cycles, showing an excellent cycling stability (Figure 7(f)). Excellent charge/discharge cycle stability and multicolor electrochromic properties make TPA-bpy the promising candidate for electrochromic supercapacitors. Compared with the reported viologen-based supercapacitors, the supercapacitors containing TPA-bpy has a wider voltage window and good stability (Table S7). Therefore, in the next work, we will combine TPA-bpy with non-electrochromic supercapacitor materials (e.g., conductive polymers, hydroxides or transition metal oxides) to produce flexible electrochromic supercapacitors with high energy density. TPA-bpy exhibits energy storage characteristics, mainly due to the introduction of packing-disruptive and three-dimensional triarylamine groups into 4,4'-bipyridine, which not only resulted in the enhancement of solubility (Table S5) but also avoided concentration quenching effectively due to π - π interactions among TPA-bpy molecules [35–37].

4 Conclusions

In this work, we synthesized novel symmetric viologens (TPA-bpy and CZ-bpy) as electroactive materials for electrochromic and electroluminescent bi-functional devices. Although they both showed rapid response time, good optical contrast, and high coloration efficiency, TPA-bpy ex-

hibited electrochemical storage properties superior to CZ-bpy due to its more excellent solubility and film-formation ability. Supercapacitors containing TPA-bpy exhibited a wide voltage window (0–2.0 V), long discharge time (230.3 s at 0.01 mA cm^{-2}), and 90% capacitance retention after 6,000 charge/discharge cycles. Meanwhile, the supercapacitor's charge and discharge status was accompanied by a color change from purple to yellow. This work provided an effective approach to fabricate multifunctional optoelectronic devices. In the future, more efforts will be made to combine TPA-bpy with transition metal oxides, hydroxides or conductive polymers, which show non-electrochromic and excellent energy storage properties, to obtain new excellent electrochromic supercapacitor materials.

Acknowledgements This work was supported by the National Funds for Distinguished Young Scientists (61825503), the National Natural Science Foundation of China (61775101, 61804082), the Priority Academic Program Development of Jiangsu Higher Education Institutions (YX030003), Natural Science Foundation of Jiangsu Higher Education Institutions (18KJB430021), the China Postdoctoral Science Foundation Funded Project (2018M642286), Jiangsu Planned Projects for Postdoctoral Research Funds (2019K047A), Natural Science Foundation of Jiangsu Province of China (BK20180760), and Science Foundation of Nanjing University of Posts and Telecommunications (NY217142).

Conflict of interest The authors declare no conflict of interest.

Supporting information The supporting information is available online at <http://chem.scichina.com> and <http://link.springer.com/journal/11426>. The supporting materials are published as submitted, without typesetting or editing. The responsibility for scientific accuracy and content remains entirely with the authors.

- Chen J, Wang Z, Chen Z, Cong S, Zhao Z. *Nano Lett*, 2020, 20: 1915–1922
- An T, Ling Y, Gong S, Zhu B, Zhao Y, Dong D, Yap LW, Wang Y, Cheng W. *Adv Mater Technol*, 2019, 4: 1800473
- Yun TG, Park M, Kim DH, Kim D, Cheong JY, Bae JG, Han SM, Kim ID. *ACS Nano*, 2019, 13: 3141–3150
- Gao W, Singh N, Song L, Liu Z, Reddy ALM, Ci L, Vajtai R, Zhang Q, Wei B, Ajayan PM. *Nat Nanotech*, 2011, 6: 496–500
- Poonam , Sharma K, Arora A, Tripathi SK. *J Energy Storage*, 2019, 21: 801–825
- Xia X, Ku Z, Zhou D, Zhong Y, Zhang Y, Wang Y, Huang MJ, Tu J, Fan HJ. *Mater Horiz*, 2016, 3: 588–595
- Zhou D, Xie D, Shi F, Wang DH, Ge X, Xia XH, Wang XL, Gu CD, Tu JP. *J Colloid Interface Sci*, 2015, 460: 200–208
- Zhou D, Xie D, Xia X, Wang X, Gu C, Tu J. *Sci China Chem*, 2017, 60: 3–12
- Zhang J, Cai G, Zhou D, Tang H, Wang X, Gu C, Tu J. *J Mater Chem C*, 2014, 2: 7013–7021
- Zhong Y, Xia X, Mai W, Tu J, Fan HJ. *Adv Mater Technol*, 2017, 2: 1700182
- Wang R, Yao M, Niu Z. *InfoMat*, 2019, 2: 113–125
- Cai G, Wang J, Lee PS. *Acc Chem Res*, 2016, 49: 1469–1476
- Yan J, Li S, Lan B, Wu Y, Lee PS. *Adv Funct Mater*, 2020, 30: 1902564
- Sun P, Deng Z, Yang P, Yu X, Chen Y, Liang Z, Meng H, Xie W, Tan S, Mai W. *J Mater Chem A*, 2015, 3: 12076–12080
- Qin S, Zhang Q, Yang X, Liu M, Sun Q, Wang ZL. *Adv Energy Mater*, 2018, 8: 1800069

- 16 Wang Y, Song Y, Xia Y. *Chem Soc Rev*, 2016, 45: 5925–5950
- 17 Wang F, Wu X, Yuan X, Liu Z, Zhang Y, Fu L, Zhu Y, Zhou Q, Wu Y, Huang W. *Chem Soc Rev*, 2017, 46: 6816–6854
- 18 Dubal DP, Chodankar NR, Kim DH, Gomez-Romero P. *Chem Soc Rev*, 2018, 47: 2065–2129
- 19 Yuksel R, Ekber A, Turan J, Alpugan E, Hacioglu SO, Toppare L, Cirpan A, Gunbas G, Unalan HE. *Electroanalysis*, 2018, 30: 266–273
- 20 Wang L, Sun S, He Y, He N, Zhang F, Yao Y, Zhang B, Zhuang X, Chen Y. *Eur Polym J*, 2018, 98: 125–136
- 21 Mortimer RJ. *Annu Rev Mater Res*, 2011, 41: 241–268
- 22 Luo J, Hu B, Debruler C, Liu TL. *Angew Chem Int Ed*, 2018, 57: 231–235
- 23 Li G, Zhang B, Wang J, Zhao H, Ma W, Xu L, Zhang W, Zhou K, Du Y, He G. *Angew Chem Int Ed*, 2019, 58: 8468–8473
- 24 Reus C, Stolar M, Vanderkley J, Nebauer J, Baumgartner T. *J Am Chem Soc*, 2015, 137: 11710–11717
- 25 Stolar M, Borau-Garcia J, Toonen M, Baumgartner T. *J Am Chem Soc*, 2015, 137: 3366–3371
- 26 Janoschka T, Martin N, Hager MD, Schubert US. *Angew Chem Int Ed*, 2016, 55: 14427–14430
- 27 Hu B, DeBruler C, Rhodes Z, Liu TL. *J Am Chem Soc*, 2017, 139: 1207–1214
- 28 Beladi-Mousavi SM, Sadaf S, Mahmood AM, Walder L. *ACS Nano*, 2017, 11: 8730–8740
- 29 Shah KW, Wang SX, Soo DXY, Xu J. *Polymers*, 2019, 11: 1839
- 30 Neo WT, Ye Q, Chua SJ, Xu J. *J Mater Chem C*, 2016, 4: 7364–7376
- 31 Chua MH, Zhu Q, Shah KW, Xu J. *Polymers*, 2019, 11: 98
- 32 Li J, Lepadatu AM, Zhu Y, Ciobanu M, Wang Y, Asaftei SC, Oupický D. *Bioconjugate Chem*, 2014, 25: 907–917
- 33 Zhu Z, Moore JS. *J Org Chem*, 2000, 65: 116–123
- 34 Hsiao SH, Liou GS, Wang HM. *J Polym Sci A Polym Chem*, 2009, 47: 2330–2343
- 35 Wang HM, Hsiao SH. *J Polym Sci Part A-Polym Chem*, 2014, 52: 272–286
- 36 Yen HJ, Liou GS. *J Mater Chem*, 2010, 20: 9886–9894
- 37 Wang HM, Hsiao SH. *J Mater Chem C*, 2014, 2: 1553–1564
- 38 Usluer O, Demic S, Egbe DAM, Birckner E, Tozlu C, Pivrikas A, Ramil AM, Sariciftci NS. *Adv Funct Mater*, 2010, 20: 4152–4161
- 39 Warde U, Sekar N. *J Fluoresc*, 2018, 28: 293–309
- 40 Schwabe T. *J Phys Chem B*, 2015, 119: 10693–10700
- 41 Striepe L, Baumgartner T. *Chem Eur J*, 2017, 23: 16924–16940
- 42 Oh H, Seo DG, Yun TY, Kim CY, Moon HC. *ACS Appl Mater Interfaces*, 2017, 9: 7658–7665
- 43 Sathyamoorthi S, Kanagaraj M, Kathiresan M, Suryanarayanan V, Velayutham D. *J Mater Chem A*, 2016, 4: 4562–4569
- 44 Cai G, Wang X, Cui M, Darmawan P, Wang J, Eh ALS, Lee PS. *Nano Energy*, 2015, 12: 258–267
- 45 Zhong Y, Zhang X, He Y, Peng H, Wang G, Xin G. *Adv Funct Mater*, 2019, 28: 1801998
- 46 Peng H, Zhong Y, Zhang X, He Y, Wang G. *Langmuir*, 2018, 34: 15245–15252
- 47 Zhang CJ, Anasori B, Seral-Ascaso A, Park SH, McEvoy N, Shmeliov A, Duesberg GS, Coleman JN, Gogotsi Y, Nicolosi V. *Adv Mater*, 2017, 29: 1702678